Clogging and jamming transitions in periodic obstacle arrays

H. T. Nguyen, C. Reichhardt, and C. J. Olson Reichhardt

Phys. Rev. E **95**, 030902 — Published 29 March 2017
DOI: 10.1103/PhysRevE.95.030902

Clogging and Jamming Transitions in Periodic Obstacle Arrays

H.T. Nguyen[1,2], C. Reichhardt[1], and C. J. Olson Reichhardt[1]
[1] *Theoretical Division, Los Alamos National Laboratory, Los Alamos, New Mexico 87545 USA*
[2] *Department of Physics, University of South Florida, Tampa, Florida 33620 USA*
(Dated: February 9, 2017)

We numerically examine clogging transitions for bidisperse disks flowing through a two dimensional periodic obstacle array. We show that clogging is a probabilistic event that occurs through a transition from a homogeneous flowing state to a heterogeneous or phase separated jammed state where the disks form dense connected clusters. The probability for clogging to occur during a fixed time increases with increasing particle packing and obstacle number. For driving at different angles with respect to the symmetry direction of the obstacle array, we show that certain directions have a higher clogging susceptibility. It is also possible to have a size-specific clogging transition in which one disk size becomes completely immobile while the other disk size continues to flow.

A loose collection of particles such as grains or bubbles can exhibit a transition from a flowing liquidlike state to a non-flowing or jammed state as a function of increasing density, where the density ϕ_j at which the system jams is referred to as Point J [1–3]. Jamming has been extensively studied in bidisperse two-dimensional (2D) packings of frictionless disks, for which $\phi_j \approx 0.844$, and where the system density is uniform at the jamming transition [1, 2, 4]. Related to jamming is the phenomenon of clogging, as observed in the flow of grains [5–8] or bubbles [9] through an aperture at the tip of a hopper. The clogging transition is a probabilistic process in which, for a fixed grain size, the probability of a clogging event occurring during a fixed time interval increases with decreasing aperture size. A general question is whether a system can exhibit features of both jamming and clogging. For example, in a system containing quenched disorder such as pinning or obstacles, jammed or clogged configurations can be created by a combination of particles that are directly immobilized in a pinning site as well as other particles that are indirectly immobilized through contact with obstacles or pinned particles. In many systems where pinning effects arise, such as for superconducting vortices or charged particles, the particle-particle interactions are long range, and there is no well defined areal coverage density at which the system can be said to jam [10], so a more ideal system to study is an assembly of hard disks with strictly short range particle-particle interactions. Previous studies have described the effect of a random pinning landscape on transport in a 2D sample of bidisperse hard disks [11], while in other work on the effect of obstacles, the density at which jamming occurs decreases when the number of pinning sites or obstacles increases [12, 13].

Here we examine a 2D system of bidisperse frictionless disks flowing through a square periodic obstacle array with lattice constant a composed of immobile disks. The total disk density ϕ_t is defined as the area coverage of the mobile disks and the obstacles. We find that for ϕ_t far below the obstacle-free jamming density ϕ_j, the system can reach clogged configurations by forming a phase separated state consisting of a high density connected cluster surrounded by empty regions, and that the clogging probability P_c during a fixed time interval depends on both a and ϕ_t. There is also a strong dependence of P_c on the angle θ between the driving direction and the x-axis symmetry direction of the obstacle lattice, with an increase in P_c for certain incommensurate angles. Over a range of θ values we observe a novel size-dependent clogging effect in which the smaller disks become completely jammed while a portion of the larger disks continue to flow. This work is relevant for filtration processes [14–16], the flow of discrete particles in porous media [17, 18], and the flow and separation of of colloids on periodic substrates [19–22].

Model and Method— We consider a 2D square system of size $L \times L$ where $L = 60$ with periodic boundary conditions in the x and y-directions. The sample contains N_l disks of diameter $\sigma_l = 1.4$ and $N_s = N_l$ disks of diameter $\sigma_s = 1.0$, giving a size ratio of $1 : 1.4$. This same size ratio was studied in previous works examining jamming in bidisperse obstacle-free disk packings, where jamming occurs at $\phi_j = 0.844$ and is associated with a contact number of $Z = 4.0$ [1–4]. We place N_p obstacles, modeled as immobile disks of diameter $\sigma_s = 1.0$, in a square lattice with lattice constant a. The disks interact through a repulsive short range harmonic force, $\mathbf{F}^{in}_{ij} = k(\sigma_{ij} - |\mathbf{r}_{ij}|)\Theta(\sigma_{ij} - |\mathbf{r}_{ij}|)\hat{\mathbf{r}}_{ij}$ where $\sigma_{ij} = (\sigma_i + \sigma_j)/2$ is the sum of the radii of disks i and j, $\mathbf{r}_{ij} = \mathbf{r}_i - \mathbf{r}_j$, $\hat{\mathbf{r}}_{ij} = \mathbf{r}_{ij}/|\mathbf{r}_{ij}|$, and Θ is the Heaviside step function. The spring constant is set to $k = 300$ which is large enough to ensure that the overlap between disks for the largest driving force we consider remains small. To prepare the initial disk configuration, we alternately place small and large disks in the sample at randomly chosen available spaces that are not already occupied by disks or obstacles. Then we apply a constant driving force $\mathbf{F}_d$ to the mobile disks which could arise from a gravity or fluid induced flow. The dynamics for a given disk i at position $\mathbf{r}_i$ is obtained by integrating the following overdamped equation of motion, appropriate for colloidal particles or for disks on a frictional surface for which inertial effects can be neglected:

$$\eta \frac{d\mathbf{r}_i}{dt} = \sum_{i \neq j}^{N} \mathbf{F}^{in}_{ij} + \mathbf{F}_d \ . \quad (1)$$

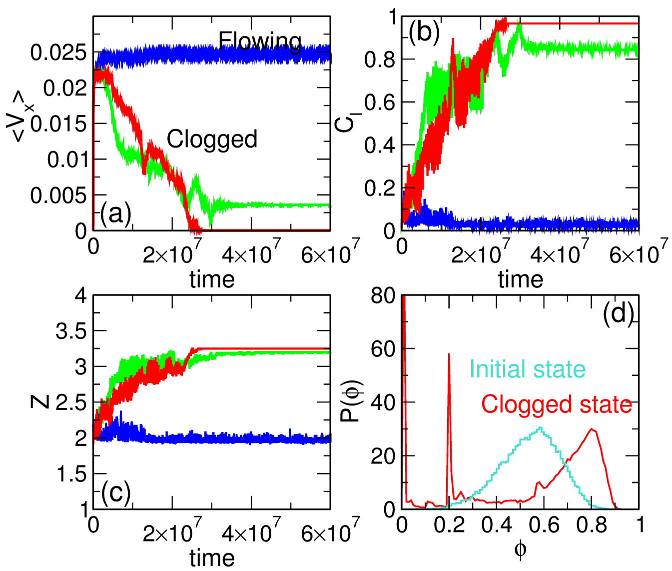

FIG. 1: (a) The average disk velocities $\langle V_x \rangle$, (b) fraction of disks in a cluster C_l, and (c) average contact number Z versus time in simulation time steps for 2D bidisperse disks moving through a square periodic obstacle array with total disk density $\phi_t = 0.54$, lattice constant $a = 3.0$, and constant external drive $F_d = 0.025$ applied in the positive x-direction. We illustrate three cases: steady state flow (blue), full clogging (red), and partial clogging (green). (d) Distribution $P(\phi)$ of local disk density ϕ in 2×2 spatial regions in the initial state (blue) and after reaching a clogged state (red), averaged over 40 clogged realizations.

Here $N = N_s + N_l + N_p$ is the total number of disks and the damping constant η determining the proportionality between the disk velocity and the forces acting on the disk is set to unity. The external driving force is given by $\mathbf{F}_d = F_d(\cos(\theta)\hat{\mathbf{x}} + \sin(\theta)\hat{\mathbf{y}})$, where θ is the angle of the driving direction with respect to the positive x axis. We take $F_d = 0.025$ but, provided F_d is sufficiently small, our results are not sensitive to the choice of F_d. In the absence of obstacles, all the disks move in the driving direction at a speed of F_d/η. The total disk density ϕ_t is the area fraction covered by the free disks and obstacles, $\phi_t = \frac{1}{4}\pi(N_l\sigma_l^2 + (N_s + N_p)\sigma_s^2)/L^2$. To quantify the clogging transition, we monitor the average velocity of the mobile disks along the x and y directions, $\langle V_{x,y} \rangle = (N_s + N_l)^{-1} \sum_{i=1}^{N_s+N_l} \mathbf{v}_i \cdot (\hat{\mathbf{x}}, \hat{\mathbf{y}})$, where $\mathbf{v}_i$ is the velocity of disk i. To ensure that the system has reached a steady state, we run all simulations for 3×10^8 simulation time steps and average the values of $\langle V_x \rangle$ and $\langle V_y \rangle$ over 10^5 simulation time steps. Generally we find that clogging occurs within 1×10^7 simulation time steps. We define P_c to be the probability that the system will reach a clogged state with $\langle V_x \rangle = 0.0$ after a total of 3×10^8 simulation time steps, and perform 100 realizations for each value of ϕ_t and a.

Results— We first consider the $\theta = 0$ case with the external drive applied along the x direction. For $a = 3.0$ we find that the clogging probability $P_c = 1.0$ for $\phi_t > 0.62$, $P_c \approx 0$ for $\phi_t < 0.52$, and $P_c = 0.31$ at $\phi_t = 0.54$. We illustrate three representative realizations of the $\phi_t = 0.54$ sample in Fig. 1(a,b,c) showing steady state flow, complete clogging, and partial clogging in which at least three-quarters of the disks are no longer moving. The plot of $\langle V_x \rangle$ versus time in Fig. 1(a) indicates that in realizations that reach a clogged state, the system does not pass instantly from a flowing to a non-flowing state, but instead exhibits a series of steps in which a progressively larger number of disks become clogged, with $\langle V_x \rangle$ continuing to diminish until it reaches zero. This behavior is different from that typically observed in hopper flows, where a single event brings the flow to a sudden and complete halt. The red curve in Fig. 1(a) contains time intervals during which the number of flowing grains, which is directly proportional to the value of $\langle V_x \rangle$, temporarily increases prior to the system reaching a final clogged state with $\langle V_x \rangle = 0$ after 2.5×10^7 simulation time steps. Since there are no thermal fluctuations or external vibrations, once the system is completely clogged, all of the dynamical fluctuations disappear and the system is permanently absorbed into a clogged state. There can also be a steady flowing state in which the disks no longer undergo any collisions and remain unclogged. When collisions produce nonequilibrium fluctuations, it is possible that if we were to consider a longer time interval, some of the flowing or partially clogged states could fully clog. In Fig. 1(b) we plot the fraction C_l of mobile disks that are in the largest connected cluster versus time, while in Fig. 1(c) we show the corresponding average disk contact number Z. For the realization that fully clogs, C_l gradually increases with time, indicating that there is a single growing cluster, while Z also increases. When $\langle V_x \rangle$ reaches zero, $C_l = 0.98$, indicating that almost all the disks have formed a single cluster, while $Z = 3.25$, which is well below the critical value $Z_c = 4.0$ expected at the obstacle-free jamming transition. In contrast, for the system that remains flowing, $\langle V_x \rangle = 0.025$, indicating that almost all of the mobile grains are freely flowing. At the same time, C_l is close to zero and $Z = 2.0$ since the disks tend to form effectively one-dimensional chains. Changing the system size changes the time required to reach a clogged state, but the nature of the clogged state remains the same.

In Fig. 2(a) we show an image of the initial uniform density disk configuration for the system in Fig. 1(a) which reaches a clogged state, while we show the final $\langle V_x \rangle = 0$ clogged state in Fig. 2(b). The mobile disks phase separate into a high density connected cluster surrounded by empty regions. In contrast, Fig. 2(c) shows a late time image of the sample from Fig. 1(a) that remains flowing. Here the overall disk density is uniform and the motion is confined in one-dimensional (1D) channels that run between the rows of obstacles. For the partially clogged sample at late times, Fig. 1(b) indicates that the cluster fraction $C_l = 0.84$ is lower than the value $C_l = 0.98$ observed in the fully clogged state,

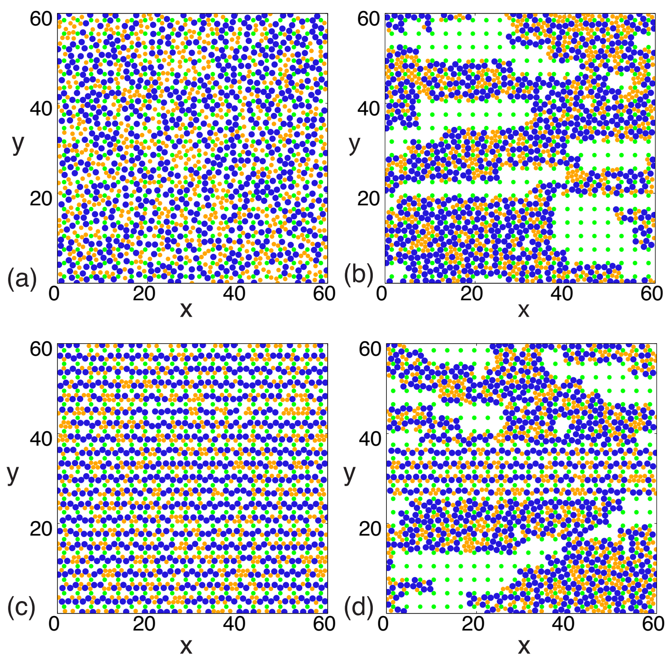

FIG. 2: Images of the obstacle locations (green circles) and the mobile disks (large disks: blue; small disks: orange) for the samples shown in Fig. 1 with $a = 3.0$ and $\phi_t = 0.54$. (a) Initial configuration of the sample that clogs. (b) Final clogged configuration of the same sample. (c) Late time configuration of the flowing sample. (d) Late time configuration of the partially clogged sample.

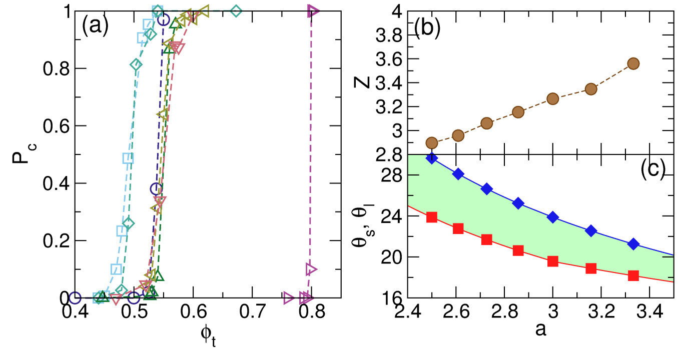

FIG. 3: (a) The clogging probability P_c vs ϕ_t for varied obstacle lattice constant $a = 2.5$ (dark blue circles), 2.609 (light blue squares), 2.727 (light green diamonds), 2.857 (dark green up triangles), 3.0 (orange left triangles), 3.158 (red down triangles), and 3.33 (magenta right triangles). (b) The average value of Z for realizations that clog vs a increases monotonically. (c) Angles θ_s (red squares) and θ_l (blue diamonds) at which x-direction channeling is lost for the small and large disks, respectively, vs a. For driving angles falling within the green shaded region, size-dependent clogging can occur.

and Fig. 2(d) shows that a large jammed cluster forms, while in the middle of the sample there is a region of uniform disk density through which the grains flow in 1D channels. The partially clogged state thus combines features of the clogged and flowing states in Fig. 2(b,c).

In Fig. 1(d) we plot the distribution $P(\phi)$ of the *local* packing density ϕ at initial and late times for a sample that reaches a clogged state. To measure ϕ, we divide the sample into squares of size 2×2 and find the area fraction of each square covered by free disks and obstacles. In the initial state, there is a peak in $P(\phi)$ centered at the total disk density of $\phi_t = 0.54$. In contrast, in the clogged state $P(\phi)$ has multiple peaks centered at $\phi = 0$ from empty regions, $\phi = 0.2$ from the obstacle density, and $\phi = 0.82$ from clogged regions, which have a density close to the free disk jamming density.

In Fig. 3(a) we plot the clogging probability P_c versus ϕ_t for samples with obstacle lattice constant ranging from $a = 2.5$ to $a = 3.33$ obtained from 100 realizations for each value of ϕ_t. When $a = 3.33$, $P_c = 0$ for $\phi_t < 0.79$, and there is a sharp increase to $P_c = 1.0$ at $\phi_t = 0.8$, indicating that when the spacing between obstacles is large, a high density of mobile particles must be introduced in order for the system to clog. We define the critical density ϕ_t^c as the value of ϕ_t at which P_c passes through $P_c = 0.5$. As a decreases, ϕ_t^c also decreases, and at $a = 2.5$, $\phi_t^c = 0.49$. For some values of a there are particular combinations of disk configurations that can better fit in the constraint of a square obstacle lattice, so ϕ_t^c does not decrease strictly monotonically with a. The combination of our finite sample size and the square symmetry of our obstacle lattice constrains us to a discrete set of values for a. When we average the contact number Z over only realizations that clog, we find a monotonic increase in Z with a, as shown in Fig. 3(b), where Z increases from $Z = 2.9$ at $a = 2.5$ to $Z = 3.6$ at $a = 3.33$. In principle, Z will approach the value $Z = 4.0$ for very large values of a or in the limit of a single obstacle when $\phi_t = \phi_j \approx 0.84$; however, the time required to reach clogged states at large a increases well beyond our simulation time window. We can compare the ratios $R_c^l = a/\sigma_l$ and $R_c^s = a/\sigma_s$ to the critical pore size R_c for hopper flow clogging identified in Ref. [23]. At $a = 3.33$ we have $R_c^l = 3.33$ and $R_c^s = 2.37$, giving an average value of $R_c = 2.85$, close to the value $R_c = 2.5$ to 3.5 for vibrated hoppers in Ref. [23] and to the value $R_c = 3.0$ for hopper flow in Ref. [24].

Directional dependence and size dependent clogging— We next consider the effect of changing the direction θ of the drive relative to the x axis symmetry direction of the square obstacle array. In Fig. 4(a) we plot P_c versus θ in samples with $\phi_t = 0.527$ and $a = 2.857$. For each value of θ, we perform 100 realizations. Here, $P_c = 0$ for $\theta = 0$, consistent with Fig. 3(a). As θ increases, a local maximum in P_c with $P_c = 0.3$ appears near $\theta = 10$. This is followed by a drop to $P_c = 0$ over the range $15^\circ < \theta < 25^\circ$, and an increase to $P_c = 0.98$ for $25^\circ \leq \theta < 40^\circ$, with a dip to $P_c = 0.72$ occurring near $\theta = 45^\circ$. Due the symmetry of the obstacle lattice, the same features repeat over the range $45^\circ < \theta < 90^\circ$. The increase of P_c near $\theta = 10^\circ$ occurs due to a breakdown of the 1D channeling

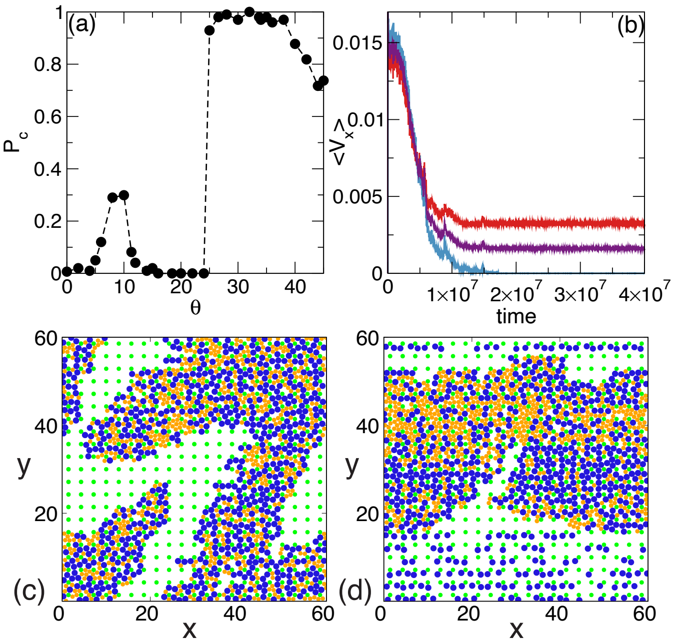

FIG. 4: (a) P_c vs θ, the driving direction angle, in samples with $\phi_t = 0.5272$ and $a = 2.857$. P_c is enhanced for $\theta > 25°$. (b) $\langle V_x \rangle$ vs time in simulation time steps for the large disks only (red), the small disks only (blue), and all disks (purple) for a driving angle of $\theta = 20°$. We find a size dependence, with only the smaller disks becoming clogged while the large disks continue to flow. (c) The disk configuration in the clogged state at $\theta = 32^0$ from panel (a). (d) The disk configuration for the size-dependent clogged state from panel (b).

that arises for the $\theta = 0°$ flow. Similarly, the dip in P_c near $\theta = 45°$ appears when the disks follow 1D flow channels along the diagonal direction. Angles such as $\theta = 0°$ and $\theta = 45°$ allow 1D channeling motion, whereas for $25° < \theta < 40°$ there is no easy flow direction so the disks are forced to collide with the obstacles, producing an increase in P_c. In Fig. 4(c) we illustrate a clogged state that is aligned with the driving angle of $\theta = 32°$.

For $20° \leq \theta \leq 24°$ we observe a size-dependent clogging behavior in which the smaller disks become completely clogged while a portion of the larger disks continue to flow. In Fig. 4(b) we plot $\langle V_x \rangle$ for the large and small disks separately and for all disks combined for a driving angle of $\theta = 20°$. After 2×10^7 simulation time steps, $\langle V_x \rangle = 0$ for the small disks, which clog completely, while the larger disks saturate to a steady state flow. This result is counter-intuitive since it might be expected that the larger disks would clog first. In Fig. 4(d) we show a snapshot of the size-dependent clogged state from Fig. 4(b). All of the smaller disks are jammed in a cluster along with a portion of the larger disks, while in the lower density regions there are a number of larger disks undergoing channeling motion along the x-direction. The size-dependent clogging can be understood as a consequence of a directional locking effect [19–22, 25] in which the flow of the larger disks remains locked to the $\theta = 0°$ direction of the obstacle lattice while the flow of the smaller disks follows the angle of the drive, which increases the chance for the smaller disks to become clogged. According to a simple geometric argument [26], the driving angle θ_m at which a disk of size σ_m ceases to channel along the x direction between obstacles and begins to move in the driving direction is given by the real root of $\tan^{-1}\left[\frac{(\cos(\theta_m)-\sin(\theta_m))}{2a/(\sigma_m+\sigma_s)-(\sin(\theta_m)+\cos(\theta_m))}\right] - \theta_m = 0$. At $a = 2.857$ the solutions are $\theta_s = 20.49°$ and $\theta_l = 24.84°$ for the small and large disks respectively, giving a window of size-dependent clogging that agrees with the numerical results. The variation of this window with a appears as a shaded region in Fig. 3(c). The directional locking effect, in which particles preferentially move along lattice symmetry directions, has been observed for colloids [19–22] and superconducting vortices [25] moving over periodic substrates. It can be used to perform particle separation by having one species lock to a symmetry direction while the other does not. In our case, the disk size that does not undergo directional locking ends up in a clogged state, suggesting that species separation by selective clogging could be a new method for particle separation.

Conclusion— We have investigated the clogging transition for a bidisperse assembly of frictionless disks moving through a two-dimensional square obstacle array. We find that the probability of clogging during a fixed time interval increases with increasing total disk density ϕ_t and decreases with the obstacle spacing a. For disk densities well below the obstacle-free jamming density, the clogged states are phase separated and consist of a connected high density jammed cluster surrounded by a low density disk-free region. In the clogged state, the contact number Z increases monotonically with decreasing obstacle density. We also find that the clogging probability has a strong dependence on the angle between the driving direction and the symmetry axes of the square obstacle array. The clogging is enhanced for incommensurate angles at which the 1D channeling flow of the disks between the obstacles is suppressed. For a window of drive angles, a size-dependent clogging effect arises in which the smaller disks become completely clogged while a portion of the larger disks remain mobile. Here the motion of the larger disks remains locked along the x-axis of the obstacle array whereas the smaller disks move in the driving direction. This suggests that selective clogging could be used as a particle separation method.

Acknowledgments

This work was carried out under the auspices of the NNSA of the U.S. DoE at LANL under Contract No. DE-AC52-06NA25396. H.N. gratefully acknowledges support from NSF Grant No. DMR-1555242.

[1] C.S. O'Hern, L.E. Silbert, A.J. Liu, and S.R. Nagel, Jamming at zero temperature and zero applied stress: The epitome of disorder, Phys. Rev. E **68**, 011306 (2003).

[2] J.A. Drocco, M.B. Hastings, C.J. Olson Reichhardt, and C. Reichhardt, Multiscaling at Point J: Jamming is a critical phenomenon, Phys. Rev. Lett. **95**, 088001 (2005).

[3] A.J. Liu and S.R. Nagel, The jamming transition and the marginally jammed solid, Annu. Rev. Condens. Matter Phys. **1**, 347 (2010).

[4] C. Reichhardt and C. J. Olson Reichhardt, Aspects of jamming in two-dimensional athermal frictionless systems, Soft Matter **10**, 2932 (2014).

[5] K. To, P.-Y. Lai, and H.K. Pak, Jamming of granular flow in a two-dimensional hopper, Phys. Rev. Lett. **86**, 71 (2001).

[6] C.C. Thomas and D.J. Durian, Geometry dependence of the clogging transition in tilted hoppers, Phys. Rev. E **87**, 052201 (2013).

[7] A. Garcimartín, J.M. Pastor, L.M. Ferrer, J.J. Ramos, C. Martín-Gómez, and I. Zuriguel, Flow and clogging of a sheep herd passing through a bottleneck, Phys. Rev. E **91**, 022808 (2015).

[8] I. Zuriguel, L.A. Pugnaloni, A. Garcimartín, and D. Maza, Jamming during the discharge of grains from a silo described as a percolating transition, Phys. Rev. E **68**, 030301(R) (2003).

[9] D. Chen, K.W. Desmond, and E.R. Weeks, Topological rearrangements and stress fluctuations in quasi-two-dimensional hopper flow of emulsions, Soft Matter **8**, 10486 (2012).

[10] C. Reichhardt and C.J. Olson Reichhardt, Depinning and nonequilibrium dynamic phases of particle assemblies driven over random and ordered substrates: a review, Rep. Prog. Phys. **80**, 026501 (2017).

[11] C.J. Olson Reichhardt, E. Groopman, Z. Nussinov, and C. Reichhardt, Jamming in systems with quenched disorder, Phys. Rev. E **86**, 061301 (2012).

[12] C. Brito, G. Parisi, and F. Zamponi, Jamming transition of randomly pinned systems, Soft Matter **9**, 8540 (2013).

[13] A.L. Graves, S. Nashed, E. Padgett, C.P. Goodrich, A.J. Liu, and J.P. Sethna, Pinning susceptibility: The effect of dilute, quenched disorder on jamming, Phys. Rev. Lett. **116**, 235501 (2016).

[14] S. Redner and S. Datta, Clogging time of a filter, Phys. Rev. Lett. **84**, 6018 (2000).

[15] F. Chevoir, F. Gaulard, and N. Roussel, Flow and jamming of granular mixtures through obstacles, EPL **79**, 14001 (2007).

[16] N. Roussel, T.L.H. Nguyen, and P. Coussot, General probabilistic approach to the filtration process, Phys. Rev. Lett. **98**, 114502 (2007).

[17] D. Liu, P.R. Johnson, and M. Elimelech, Colloid deposition dynamics in flow through porous media: Role of electrolyte concentration, Environ. Sci. Technol. **29**, 2963 (1995).

[18] F. Wirner, C. Scholz, and C. Bechinger, Geometrical interpretation of long-time tails of first-passage time distributions in porous media with stagnant parts, Phys. Rev. E **90**, 013025 (2014).

[19] P.T. Korda, M.B. Taylor, and D.G. Grier, Kinetically locked-in colloidal transport in an array of optical tweezers, Phys. Rev. Lett. **89**, 128301 (2002).

[20] M.P. MacDonald, G.C. Spalding, and K. Dholakia, Microfluidic sorting in an optical lattice, Nature (London) **426**, 421 (2003).

[21] Z. Li and G. Drazer, Separation of suspended particles by arrays of obstacles in microfluidic devices, Phys. Rev. Lett. **98**, 050602 (2007).

[22] A.M. Lacasta, J.M. Sancho, A.H. Romero, and K. Lindenberg, Sorting on periodic surfaces, Phys. Rev. Lett. **94**, 160601 (2005).

[23] C. Mankoc, A. Garcimartín, I. Zuriguel, D. Maza, and L.A. Pugnaloni, Role of vibrations in the jamming and unjamming of grains discharging from a silo, Phys. Rev. E **80**, 011309 (2009).

[24] C.C. Thomas and D.J. Durian, Intermittency and velocity fluctuations in hopper flows prone to clogging, Phys. Rev. E **94**, 022901 (2016).

[25] C. Reichhardt and F. Nori, Phase locking, devil's staircases, Farey trees, and Arnold tongues in driven vortex lattices with periodic pinning, Phys. Rev. Lett. **82**, 414 (1999).

[26] We thank the anonymous referee for bringing this geometric argument to our attention.